Characterization of Inverted-Type Organic Solar Cells with a ZnO Layer as the Electron Collection Electrode by ac Impedance Spectroscopy

Takayuki Kuwabara,* Yoshitaka Kawahara, Takahiro Yamaguchi, and Kohshin Takahashi*

Graduate School of Natural Science and Technology, Kanazawa University, Kakuma-machi, Kanazawa, Ishikawa 920-1192, Japan

ABSTRACT An inverted-type organic bulk-heterojunction solar cell inserting zinc oxide (ZnO) as an electron collection electrode, fluorine-doped tin oxide (FTO)/ZnO/[6,6]-phenyl-C_{61}-butyric acid methyl ester:regioregular poly(3-hexylthiophene) (PCBM:P3HT)/poly(3,4-ethylenedioxylenethiophene):poly(4-styrenesulfonic acid) (PEDOT:PSS)/Au, was fabricated in air and characterized by an alternating current impedance spectroscopy (IS). In the IS measurement, we observed reproducibly the electric resistance and capacitance components originating from ZnO and organic active layers, and we found that the depletion layer functioning to take out the photocurrent to the external circuit was formed in both the ZnO and PCBM:P3HT layers at the ZnO/PCBM:P3HT interface. In this letter, we propose that this IS measurement is effective for evaluating the electric properties of several layers with capacitance components in organic thin-film solar cells.

KEYWORDS: alternating current impedance spectroscopy • organic thin-film solar cells • zinc oxide

1. INTRODUCTION

Alternating current (ac) impedance spectroscopy (IS) is an electric technique used to monitor the current response when an ac voltage is applied as a function of the frequency. The IS measurement is possible to observe electric properties of a bulk and an interface that we cannot observe by a direct current (dc) method because the electric response speed for each component is different on the microscopic time scale. This method has been useful to study the electric properties of organic devices such as dye-sensitized solar cells (1−4) and organic light-emitting diodes (5, 6), and it provides mechanistic insights to improve the devices. On the other hand, research by the IS measurement on organic thin-film solar cells is relatively limited. This is probably because reasonable accuracy was not obtained for this method because of rapid performance degradation under light irradiation. Even so, a few authors have studied the electric properties of the solar cells on the basis of the IS characteristics, providing important information on the exciton dissociation at the donor/acceptor interface and charge carrier mobility and carrier lifetime in the organic active layer (7−9). However, these reports were all investigations on what we call normal-type solar cells in which the active layer was sandwiched between a transparent electrode and an Al electrode as the back electrode. In our previous studies, we developed organic solar cells using a noncorrosive Au metal as the back electrode and an indium−tin oxide (ITO)/In or a fluorine-doped tin oxide (FTO)/titanium oxide (TiO_2 or TiO_x) as the front electrode (10−16). For example, we reported that the ITO/amorphous TiO_x/[6,6]-phenyl-C_{61}-butyric acid methyl ester:regioregular poly(3-hexylthiophene) (PCBM:P3HT)/poly(3,4-ethylenedioxylenethiophene):poly(4-styrenesulfonic acid) (PEDOT:PSS)/Au inverted-type cell showed a power conversion efficiency (PCE) of 2.47% and the performance of the cells with sealing was about the same after continuous light irradiation for 120 h in an ambient atmosphere (15). Even without sealing, this solar cell maintained its performance after continuous light irradiation for 20 h. Thus, we have the techniques required to fabricate the organic thin-film solar cells with reasonable performance and stability, although not very excellent. Many papers using chemically stable n-type semiconductor TiO_2 (15−21), ZnO (22−25) or ZnS (26) as an electron collection layer in the organic thin-film solar cells have been previously reported. However, the electric properties of the inverted-type solar cells could not be understood sufficiently yet, although we recently reported the investigation by the IS measurement on this type of solar cell inserting a ZnS layer as an electron collection electrode (26). In this letter, we report the photocurrent−voltage (I−V) and IS characteristics of inverted-type bulk-heterojunction organic solar cells abbreviated as FTO/ZnO/PCBM:P3HT/PEDOT:PSS/Au, named the ZnO cell, in order to gain insight into the resistance component of each layer.

2. EXPERIMENTS

A ZnO cell was fabricated in air as follows: a total of 157 mg of zinc acetate was dissolved in 1 mL of 2-methoxyethanol

* Corresponding author. Tel: +81-76-234-4770. Fax: +81-76-234-4800. E-mail: tkuwa@t.kanazawa-u.ac.jp.

Received for review June 30, 2009 and accepted September 11, 2009

DOI: 10.1021/am900446x

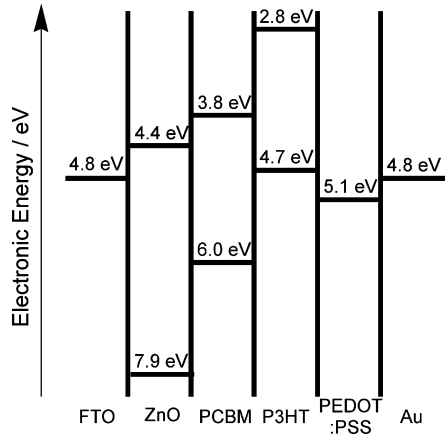

FIGURE 1. Energy-level diagram showing the work functions and the HOMO−LUMO energies of the component materials.

containing 4 % ethanolamine by weight, with this solution being used as a ZnO precursor solution (27, 28). In order to prepare a ZnO film, the precursor solution was spin-coated onto a FTO substrate (Asahi Glass A110U80, sheet resistance; 12 Ω/□) at 2000 rpm and the coated substrate was heated on a hot plate for 1 h at 250 °C. Subsequently, a mixed chlorobenzene solution of P3HT and PCBM (P3HT:PCBM = 5:4 by weight) was spin-coated onto the FTO/ZnO substrate at 700 rpm. Further, a PEDOT:PSS dispersion solution was spin-coated onto the blend film at 6000 rpm. A Au metal as the back electrode was vacuum-deposited at 2×10^{-3} Pa on the PEDOT:PSS film. The thicknesses of the ZnO film, the blended film, and the PEDOT:PSS film were 60, 250, and 80 nm, respectively. Finally, the device was heated at 150 °C for 5 min. The cell area of the solar cell was restricted to 1.0 cm^2 by depositing the Au electrode using a shadow mask. The *I*−*V* curves were measured by a Hokuto Denko HZ-5000 at a scan rate of 5 V min^{-1} in linear sweep voltammetry under a solar simulated light AM 1.5G, 100 mW cm^{-2}, by a SAN-EI ELECTRIC XES-502S solar simulator calibrated by an EKO MS-601 pyranometer equipped with a silicon diode. The IS measurements were implemented using a Hewlett-Packard precision LCR meter 4284A. The frequency range was from 20 Hz to 1 MHz, and the magnitude of the alternative signal was 5 mV. The obtained data were fitted with Scribner Associates Z-View software v2.6 in terms of appropriate equivalent circuits. Ionization potentials for P3HT, PCBM, PEDOT:PSS, FTO, and Au were estimated by a Riken Keiki model AC-2 and band-gap energies for P3HT and PCBM by a Hitachi U-3310 spectrophotometer, and the energy-level diagram of the component materials in the ZnO cell is shown in Figure 1. All measurements were carried out in an ambient atmosphere with an unsealed ZnO cell.

3. RESULTS AND DISCUSSION

Figure 2a and the inset show dark *I*−*V* curves of the ZnO cell before (blue curve) and just after light irradiation (red curve), with clear rectification characteristics being obtained. Just after irradiation of the AM 1.5G sunlight, the forward bias current in the dark under a range of 0.5−1.0 V increased from 6.5 to 10 times when compared with that before irradiation. The increase indicates that photoproduced carriers remained in the ZnO cell even after light irradiation. However, when the ZnO cell was left for several days in the dark after light irradiation, its forward bias current became small, being consistent with the blue curve before irradiation.

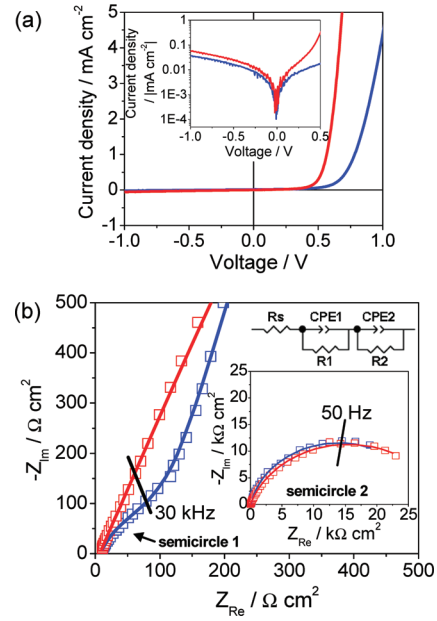

FIGURE 2. (a) *I*−*V* curves of the ZnO-inserted solar cell in the dark before (blue) and just after light irradiation (red). The inset shows the semilog plots of the *I*−*V* curves of the ZnO cell under the same conditions. (b) Typical Nyquist plots for the ZnO cell at zero bias. The open symbols in the Nyquist plots were obtained for the cells in the dark before (blue) and just after light irradiation (red), respectively. The solid lines indicate fitting curves calculated by an equivalent circuit shown in the inset. Another inset shows the full plots of the Nyquist plots containing two semicircles. Rs = series resistance consisting of ohmic components. CPE1 and CPE2 = capacitances. R1 and R2 = resistances.

In order to investigate such a change of the internal resistance in the ZnO cell, an IS measurement was carried out under the same cell conditions as those in the *I*−*V* measurement. Figure 2b shows the Nyquist plots for the ZnO cell at zero bias in the dark. Two semicircles were observed at higher frequency of more than 30 kHz and at lower frequency of less than 30 kHz, being denoted semicircles 1 and 2, respectively. That is, the ac response of semicircle 2 in the low-frequency range was slower than that of another semicircle 1 in the high-frequency range. Further, the plots were analyzed using an equivalent circuit, as shown in the inset of Figure 2b, showing reasonable concordance with a simulated curve. The Rs represents the series resistance consisting of ohmic components. R1 and R2 are resistance components forming a parallel circuit with constant phase elements (CPE1 and CPE2). Further, CPE1 and CPE2 are roughly equal to differential electric capacitances because there was almost no depression of semicircles. The R2 value of semicircle 2 obtained from the fitting data remained ca. 30 kΩ cm^2 before and just after light irradiation, whereas the R1 value of semicircle 1 decreased from 104 Ω cm^2 before irradiation down to 29 Ω cm^2 just after irradiation. In addition, when the *I*−*V* and IS measurements of the ZnO cell were carried out in the dark just after irradiation using light through a UV (<440 nm) cut filter to eliminate the influence of the UV component being contained in the simulated sunlight, the forward bias current and the R1 value were nearly equal to those before irradiation. (not shown). Hence, this component is attributed to the electric resistance

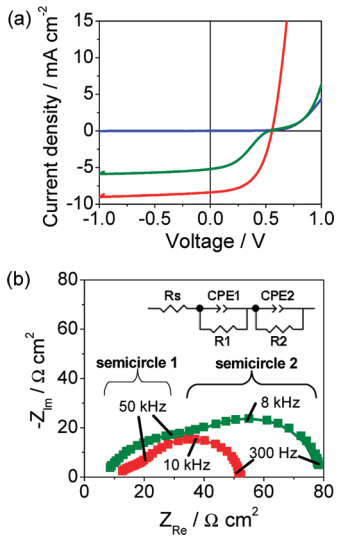

FIGURE 3. (a) *I*−*V* curves of the ZnO-inserted solar cell in the dark (blue) and under light (red) and UV cut light irradiation (green). (b) Typical Nyquist plot for the ZnO cell at zero bias under light irradiation with (red) and without a UV light (<440 nm) cut filter (green). The Nyquist plot was obtained for the cell under light irradiation. The solid line indicates the fitting curve calculated by the equivalent circuit in the inset.

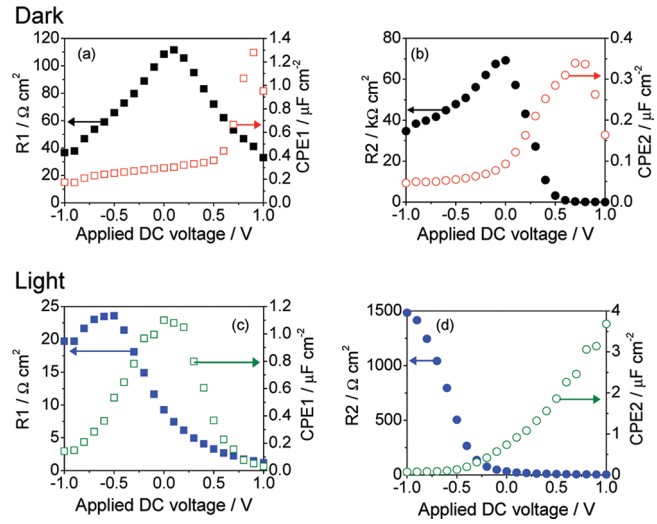

FIGURE 4. Dependence of the R and CPE values of the ZnO-inserted solar cells on the dc bias voltage in the dark (a and b) and under light irradiation (c and d): plots for a higher-frequency component (a and c); plots for a lower-frequency component (b and d).

of the ZnO layer showing a photoconductive property by UV light irradiation (29).

Figure 3a shows the photo *I*−*V* curve of the ZnO cell under light irradiation with (85.7 mW cm^{-2}) and without a UV light cut filter (100 mW cm^{-2}). The performance without the filter showed a short-circuit photocurrent (J_{sc}) of 8.39 mA cm^{-2}, an open-circuit voltage (V_{oc}) of 0.56 V, a fill factor (FF) of 0.53, and a PCE of 2.49%; see the red curve. When we reduced the intensity of the AM1.5G solar simulated light from 100 to 85.7 mW cm^{-2}, the PCE value increased up to 2.62% by improving slightly the FF. This is perhaps because an *I*−*R* loss, which is caused by the internal resistance of the ZnO cell, decreased because of the decrease of the photocurrent density, whereas the performance with the UV light cut filter showed a J_{sc} of 5.21 mA cm^{-2}, a V_{oc} of 0.53 V, a FF of 0.36, and a PCE of 1.16%; see the green curve. This PCE value with the filter decreased by ca. 56% compared to the PCE (2.62%) of the former. This is attributed to the large decrease of the FF value, which was derived from an increase in the charge-transport resistance of the ZnO layer. This result suggests that a photoconduction of ZnO was not almost observed by cutting the UV light (29). Figure 3b shows the Nyquist plots of the ZnO cell under light irradiation with (85.7 mW cm^{-2}) and without a UV light cut filter (100 mW cm^{-2}). The plots under light irradiation showed two semicircles at higher frequency of more than 50 kHz and at lower frequency of less than 50 kHz, similar to those in the dark. These plots were substantially consistent with the fitting curve simulated by an equivalent circuit, as shown in the inset of Figure 3b. The R1 and R2 values without the filter were estimated to be 17 and 34 Ω cm^2 from the fitting curve, respectively. The R2 value under irradiation was much lower by 3 orders of magnitude than that (30 kΩ cm^2) in the dark. This large decrease in the resistance component is attributed to a large increase of the photoconductive carriers in the PCBM:P3HT film by light irradiation. This result indicates that the component in the low-frequency range is derived from the organic active layer. In addition, the R1 and R2 values with the filter were estimated to be 32 and 38 Ω cm^2 from the fitting curve, respectively. The R1 value with the filter increased by 2 times compared with that (17 Ω cm^2) without the filter. This suggests that electron carriers in the ZnO layer decreased by cutting UV light, being consistent with the electric properties of the ZnO layer suggested by dark *I*−*V* curves and IS measurements shown in Figure 2.

In order to analyze the ac impedance characteristics in more detail, a constant dc bias voltage from −1.0 to +1.0 V was applied across the Au (positive) and FTO (negative) electrodes during each IS measurement. Figure 4a shows plots of the R1 and CPE1 values of the ZnO cell on the dc applied voltage in the dark. The R1 value in the dark was 33 Ω cm^2 at 1 V of applied voltage, while this value increased to 112 Ω cm^2 at 0 V. Furthermore, the rapid decrease in CPE1 was observed with decreasing dc voltage from 0.9 to 0.5 V. These changes are attributed to the fact that the depletion layer with low carrier density was gradually formed in the ZnO layer with decreasing dc voltage from 1 to 0 V. On the other hand, the decrease of R1 was observed by applying a dc voltage of less than 0 V because of the leak current of the ZnO cell; see the inset in Figure 2a. Similarly, the R2 value in the dark increased when the dc bias voltage applied was decreased from 0.6 to 0 V, as shown in Figure 4b. Simultaneously, CPE2 also decreased by applying a bias voltage of less than 0.6 V. The behavior suggests the formation of the depletion layer in the PCBM:P3HT layer by applying a dc bias voltage of less than 0.6 V. Because an electric field formed in the depletion layer forced ZnO, PCBM, and P3HT existing in the layer to polarize, the polarizability of these materials decreased, and as a result, CPE1 and CPE2 decreased. That is, the responsive polarization capacities are limited by the external bias.

By contrast, the dependence of R1, R2, CPE1, and CPE2 under light irradiation on the applied dc voltage shifted to a

significantly negative direction compared with those in the dark, as shown in Figure 4c,d. These results show that the electric-field profile of these depletion layers changed reasonably because many photocarriers were produced in the ZnO and PCBM:P3HT layers under light irradiation. Furthermore, the maximum of R2 observed at 0 V in the dark disappeared under irradiation; see Figure 4b,d. This is probably because the leak current in the ZnO cell at less than 0 V of the dc bias voltage was very small compared with the photocurrent.

4. CONCLUSION

The photoelectric properties of the inverted-type organic thin-film solar cells with ZnO as an electron collection layer were studied by photo $I-V$ and IS measurements. The photo $I-V$ measurement gave a PCE of 2.49%, and the IS measurements in the dark and under light irradiation gave Nyquist plots consisting of two components. We decided that the component in the low-frequency range originated from the organic active layer and another in the high-frequency range was derived from the ZnO layer. According to this result, it was proven that the depletion layer functioning to take out the photocurrent to the external circuit was formed in both of the ZnO and PCBM:P3HT layers at the ZnO/PCBM:P3HT interface. In this way, photoelectric properties of the organic thin-film solar cells were analyzed more apparently by introducing the photo IS measurement. Applying the IS method to understand the properties of organic thin-film solar cells in detail will give very useful insights toward the performance improvement, but we have not used this excellent method completely yet. We are extensively investigating organic solar cells using other n-type semiconductors to develop a high-performance and long-lifetime device for the practical use.

Acknowledgment. This work was supported by a Grant-in-Aid for Young Scientists (A) from the Ministry of Education, Culture, Sports, Science and Technology (Grant 21686011).

REFERENCES AND NOTES

(1) Han, L.; Koide, N.; Chiba, Y.; Mitate, T. *Appl. Phys. Lett.* **2004**, *84*, 2433.
(2) Wang, Q.; Moser, J.-E.; Gratzel, M. *J. Phys. Chem. B* **2005**, *109*, 14945.
(3) Bisquert, J.; Gratzel, M.; Wang, Q.; Fabregat-Santiago, F. *J. Phys. Chem. B* **2006**, *110*, 11284.
(4) Wang, Q.; Ito, S.; Gratzel, M.; Fabregat-Santiago, F.; Mora-Sero, I.; Bisquert, J.; Bessho, T.; Imai, H. *J. Phys. Chem. B* **2006**, *110*, 25210.
(5) Jaiswal, M.; Menon, R. *Appl. Phys. Lett.* **2006**, *88*, 123504.
(6) Hsiao, C.-C.; Hsiao, A.-E.; Chen, S.-A. *Adv. Mater.* **2008**, *20*, 1982.
(7) Glatthaar, M.; Mingirulli, N.; Zimmermann, B.; Ziegler, T.; Kern, R.; Niggemann, M.; Hinsch, A.; Gombert, A. *Phys. Status Solidi A* **2005**, *202*, R125.
(8) Garcia-Belmonte, G.; Munar, A.; Barea, E. M.; Bisquert, J.; Ugarte, I.; Pacios, R. *Org. Electron.* **2008**, *9*, 847.
(9) Bisquert, J.; Garcia-Belmonte, G.; Munar, A.; Sessolo, M.; Soriano, A.; Bolink, H. J. *Chem. Phys. Lett.* **2008**, *465*, 57.
(10) Takahashi, K.; Nakajima, I.; Imoto, K.; Yamaguchi, T.; Komura, T.; Murata, K. *Sol. Energy Mater. Sol. Cells* **2003**, *76*, 115.
(11) Nakamura, J.-i.; Yokoe, C.; Murata, K.; Takahashi, K. *J. Appl. Phys.* **2004**, *96*, 6878.
(12) Nakamura, J.-i.; Suzuki, S.; Takahashi, K.; Yokoe, C.; Murata, K. *Bull. Chem. Soc. Jpn.* **2004**, *77*, 2185.
(13) Takahashi, K.; Seto, K.; Yamaguchi, T.; Nakamura, J.-i.; Yokoe, C.; Murata, K. *Chem. Lett.* **2004**, *33*, 1042.
(14) Takahashi, K.; Takano, Y.; Yamaguchi, T.; Nakamura, J.-i.; Yokoe, C.; Murata, K. *Synth. Met.* **2005**, *155*, 51.
(15) Kuwabara, T.; Nakayama, T.; Uozumi, K.; Yamaguchi, T.; Takahashi, K. *Sol. Energy Mater. Sol. Cells* **2008**, *92*, 1476.
(16) Kuwabara, T.; Sugiyama, H.; Yamaguchi, T.; Takahashi, K. *Thin Solid Films* **2009**, *517*, 3766.
(17) Hayakawa, A.; Yoshikawa, O.; Fujieda, T.; Uehara, K.; Yoshikawa, S. *Appl. Phys. Lett.* **2007**, *90*, 163517.
(18) Kim, J. Y.; Lee, K.; Coates, N. E.; Moses, D.; Nguyen, T.-Q.; Dante, M.; Heeger, A. J. *Science* **2007**, *317*, 222.
(19) Mor, G. K.; Shankar, K.; Paulose, M.; Varghese, O. K.; Grimes, C. A. *Appl. Phys. Lett.* **2007**, *91*, 152111.
(20) Steim, R.; Choulis, S. A.; Schilinsky, P.; Brabec, C. J. *Appl. Phys. Lett.* **2008**, *92*, 093303.
(21) Schmidt, H.; Flugge, H.; Winkler, T.; Bulow, T.; Riedl, T.; Kowalsky, W. *Appl. Phys. Lett.* **2009**, *94*, 243302.
(22) Takahashi, K.; Nishi, T.; Suzaka, S.; Sigeyama, Y.; Yamaguchi, T.; Nakamura, J.-i.; Murata, K. *Chem. Lett.* **2005**, *34*, 768.
(23) Sahin, Y.; Alem, S.; de Bettignies, R.; Nunzi, J.-M. *Thin Solid Films* **2005**, *476*, 340.
(24) Hau, S. K.; Yip, H.-L.; Ma, H.; Jen, A. K.-Y. *Appl. Phys. Lett.* **2008**, *93*, 233304.
(25) Takanezawa, K.; Tajima, K.; Hashimoto, K. *Appl. Phys. Lett.* **2008**, *93*, 063308.
(26) Kuwabara, T.; Nakamoto, M.; Kawahara, Y.; Yamaguchi, T.; Takahashi, K. *J. Appl. Phys.* **2009**, *105*, 124513.
(27) Aslan, M. H.; Oral, A. Y.; Mensur, E.; Gul, A.; Basaran, E. *Sol. Energy Mater. Sol. Cells* **2004**, *82*, 543.
(28) Lira-Cantu, M.; Krebs, F. C. *Sol. Energy Mater. Sol. Cells* **2006**, *90*, 2076.
(29) Goncalves, G.; Pimentel, A.; Fortunato, E.; Martins, R.; Queiroz, E. L.; Bianchi, R. F.; Faria, R. M. *J. Non. Cryst. Solids* **2006**, *352*, 1444.

AM900446X